Lattice dynamics across the magnetic transition in $(Mn,Fe)_{1.95}(P,Si)$

D. Bessas,[1,*] M. Maschek,[1] H. Yibole,[1] J.-W. Lai,[1] S. M. Souliou,[2] I. Sergueev,[3] A. I. Dugulan,[1] N. H. van Dijk,[1] and E. Brück[1]

[1]*Fundamental Aspects of Materials and Energy, Department of Radiation Science and Technology, Delft University of Technology, Mekelweg 15, 2629 JB Delft, The Netherlands*

[2]*European Synchrotron Radiation Facility, F-38043 Grenoble, France*

[3]*FS-PE, Deutsches Elektronen-Synchrotron (DESY), D-22607 Hamburg, Germany*

(Received 3 January 2018; published 14 March 2018)

The lattice dynamics in $MnFe_{0.95}Si_{0.50}P_{0.50}$ were investigated experimentally using ^{57}Fe nuclear inelastic scattering and inelastic x-ray scattering across the first-order magnetic transition which occurs close to room temperature. The lattice dynamics characterization was supported by a macroscopic magnetic characterization, an x-ray diffraction study, and a hyperfine interactions characterization using Mössbauer spectroscopy. The Fe specific and the x-ray generalized density of phonon states were obtained both in the ferromagnetic and in the paramagnetic state. A prominent shift, 2 meV at 20 meV, in the x-ray generalized density of phonon states across the first-order magnetic transition, that involves vibrations with essentially Fe character, is revealed corroborated by a change in the local environment quantified in the isomer shift and the quadrupole splitting. Above 35 meV the vibrational modes are practically insensitive to the magnetic transition. The entropy change induced by a 1 T magnetic field across the magnetic transition, ∼10 J/K/kg, is only a fraction of the Fe vibrational entropy change, 62(21) J/K/kg.

DOI: 10.1103/PhysRevB.97.094303

I. INTRODUCTION

Magnetic materials relevant to caloric applications comprise a set of compounds which exhibit a strong variation of magnetization with temperature and a strong coupling of magnetization to an external magnetic field with or without the release of latent heat. Integrating such an effect into a cycle may lead to technological applications such as magnetic heat pumps, magnetic refrigerators [1], or thermomagnetic motors for waste heat recovery [2].

The quest for materials suitable for magnetocaloric applications close to room temperature resulted in systems beyond the archetypal Gd metal, such as: Fe-Rh alloys [3], $Gd_5(Ge,Si)_4$ [4], Fe_2P [5], $La(Fe,Si)_{13}$ systems [6], Heusler alloys [7], perovskite [8], and antiperovksite type structures [9]. Besides the technological interest, systems which show an enhanced magnetocaloric effect are also attractive for fundamental research due to the synergistic phenomena relevant to the strong coupling between vibrational and magnetic degrees of freedom.

In $(Mn,Fe)_2(P,Si)$ based compounds and in $La(Fe,Si)_{13}$ systems the magnetic transition is not accompanied by any structural transition. The magnetic transition under a magnetic field of 1 T is sharp and results in a large isothermal magnetic entropy change of ∼10 J/K/kg and a sizable adiabatic temperature change of ∼3 K [10,11]. In the absence of a magnetostructural transition such an isothermal magnetic entropy and adiabatic temperature change is of inherent interest.

Earlier theoretical and experimental Fe resolved thermodynamic studies in $LaFe_{11.6}Si_{1.4}$ [12] invoked that the electronic structure and the macroscopic thermodynamic properties may be coupled and lead to a new type of itinerant electron metamagnetism. Despite the simplicity of the unit cell, i.e., cubic symmetry (space group: $Fm\bar{3}c$), further interpretation based on the vibrational properties was limited mainly because a rather featureless density of vibrational states is observed probably due to the large number of atoms, i.e., 112 atoms, in the unit cell. Moreover, the non-negligible volume change across the magnetic transition of ∼2% [13] did not allow to attribute the observed effects to a single source.

A more detailed study on $Mn_{5-x}Fe_xSi_3$ compounds with hexagonal symmetry (space group: $P6_3/mcm$) for $1 < x < 4$ revealed a very broad temperature region of the magnetic transition indicative of a second-order character [14]. The elemental contribution in the lattice dynamics could be separated in the crystallographic sites occupied by Mn and Fe. Nevertheless, a magnetoelastic interaction is not observed in vibrational modes above 3 meV. Only a discrepancy in the extracted sound velocity at 16 meV and 3 meV is found and attributed to a strong phonon-magnon interaction below 3 meV.

Fe_2P based compounds crystallize in a hexagonal unit cell (space group: $P\bar{6}2m$). Other $3d$ transition metals like Mn [15], Co [16], Ni [17], or metalloids like Si [18], Ge [19], As [20], may substitute Fe and P, respectively, and thus tailor the functional properties without substantially changing the unit cell. There are two inequivalent Fe positions, the $3f$ (tetrahedral coordination-preferential Fe occupation) and the $3g$ (pyramidal coordination-preferential Mn occupation), and two inequivalent P positions, the $2c$ and the $1b$ (the metalloids are usually randomly distributed in these positions).

*Present address: European Synchrotron Radiation Facility, F-38043 Grenoble, France; bessasd@gmail.com

Thus, $(Mn,Fe)_2(P,Si)$ based compounds constitute an ideal playground in order to clarify the nature of magnetoelastic transition. This is not only because the unit cell is rather small, it contains only nine atoms, and the $3d$ transition metal contribution may be divided into the constituent crystallographic sites, but also because the density of vibrational states is very well structured and the high-energy modes are separated from the low-energy vibrational modes [21].

Here, we report a comprehensive lattice dynamics characterization by an experimental study of the Fe specific and the x-ray generalized density of phonon states across the first-order magnetic transition in $(Mn,Fe)_{1.95}(P,Si)$. We show that vibrational modes with an energy up to 35 meV, unlike higher energy vibrational modes, are highly sensitive to the magnetic transition. A 2 meV downshift at 20 meV is observed across the magnetic transition. We indicate that the energy shift of the vibrational modes originates mainly from redistribution of the Fe vibrational modes.

II. METHODS

The studied samples have a nominal stoichiometry of $MnFe_{0.95}Si_{0.50}P_{0.50}$. Stoichiometric quantities of high purity Mn, Fe, P, and Si powders in natural abundance were ground in a planetary ball mill for 10 h. The resulting powders were pressed into pellets and sealed in quartz ampules under 200 mbar of Ar. The samples were annealed following the procedure described in Ref. [22].

Magnetic measurements were carried out using a Quantum Design superconducting quantum interference device MPMS magnetometer.

A structural pre-characterization using x-ray diffraction was carried out. The x-ray diffraction patterns were obtained in the ferromagnetic (FM) phase at 295 K, and in the paramagnetic (PM) phase at 450 K in zero externally applied magnetic field by utilizing a PANalytical X-pert Pro diffractometer and a X'celerator real time multiple strip detector system and Cu-K_α radiation.

Transmission ^{57}Fe Mössbauer spectra were collected under the same conditions at 295 K and at 480 K using a spectrometer equipped with a sinusoidal velocity transducer utilizing a ^{57}Co(Rh) source. The velocity calibration was carried out using an α-Fe foil at room temperature. The Mössbauer spectra were fitted using the Mosswinn 4.0 program [23].

We have employed nuclear inelastic scattering (NIS) [24,25] by ^{57}Fe and inelastic x-ray scattering (IXS) using crystal analyzers. The measurements were carried out about 100 K away from the magnetic transition. The exact temperature at which the inelastic scattering spectra were collected was extracted by applying the detailed balance.

NIS measurements were carried out using an incident x-ray beam of 14.413 keV at the nuclear resonance beamline ID18 [26] of the European Synchrotron Radiation Facility (ESRF). The instrumental resolution of the spectrometer was measured simultaneously with the inelastic measurements and resulted in a full width at half maximum (FWHM) of 0.8 meV. The Fe density of phonon states (DPS) was obtained by employing the double Fourier transformation as implemented in the software DOS [27].

IXS measurements were carried out at the ID28 beamline of ESRF [28]. The energy of the incident x rays was 17.794 keV. The radiation scattered from the sample was analyzed using nine crystal analyzers. The momentum transfer resolution of each analyzer was about 0.03 $Å^{-1}$. The scattered radiation was collected in momentum transfer between 35 and 66 nm^{-1}. The values of the momentum transfer for each analyzer were selected away from Bragg peaks. The IXS data were collected for sufficiently high values and in a sufficiently large range of the momentum transfer in order to assure the validity of the incoherent approximation [29] required for the proper integration of vibrational states. The instrumental function of the spectrometer was measured separately for each analyzer using x-ray scattering from a polymethyl methacrylate (PMMA) sample at 15 K. Each analyzer was adjusted to the peak position of the static structure factor of the PMMA sample. The measured average FWHM was 3.0 meV. The total measured scattering function was obtained by summing the detected scattering function from each of the analyzers. Prior to summation the measured instrumental function of each analyzer was subtracted from the corresponding inelastic data. The efficiency of the individual analyzers did not affect the quality of incoherent approximation in a significant manner.

The total x-ray generalized DPS was obtained by employing the usual double Fourier transformation [27]. The total inelastic scattering spectrum can be scaled vertically to the absolute scale of the density probability of inelastic scattering by forcing the first moment of the spectrum to be equal to the recoil energy of a free atom [27]. However, in contrast to NIS the recoil energy of each constituent is not a well defined value. This is because the measured spectra are composed of many partial subspectra related to the different scattering angles and different masses of the constituent elements. The resulting inelastic scattering spectra were treated using a single variable parameter called effective recoil energy and the x-ray generalized density of phonon states was extracted. Two criteria were used in order to select the appropriate effective recoil energy: (i) a zero density of phonon states above 60 meV and (ii) a phonon gap between 38 and 40 meV. The obtained x-ray generalized total DPS could lead to the true total DPS provided accurate first principle calculations and heat capacity measurements, see, e.g., Ref. [30], however, this is beyond the scope of the present study.

III. RESULTS

A. Magnetic characterization

Figure 1 shows the temperature dependence of the magnetization for $MnFe_{0.95}Si_{0.50}P_{0.50}$ at an externally applied magnetic field of 1 T. The magnetization in the FM state at 5 K is above 160 Am^2/kg whereas in the PM state at 380 K, it is below 10 Am^2/kg . The heating and cooling curves depict a thermal hysteresis. A magnetic transition with a maximum slope, $-dM/dT$, of 15 $Am^2/kg/K$ is observed in cooling, and an even higher slope of 17 $Am^2/kg/K$ is observed in heating. The transition temperature, defined as the center of the $-dM/dT$ peak, is at $T_C = 351(1)$ K for cooling and at 368(1) K for heating. The inset of Fig. 1 shows isothermal magnetization data measured on the same sample with an

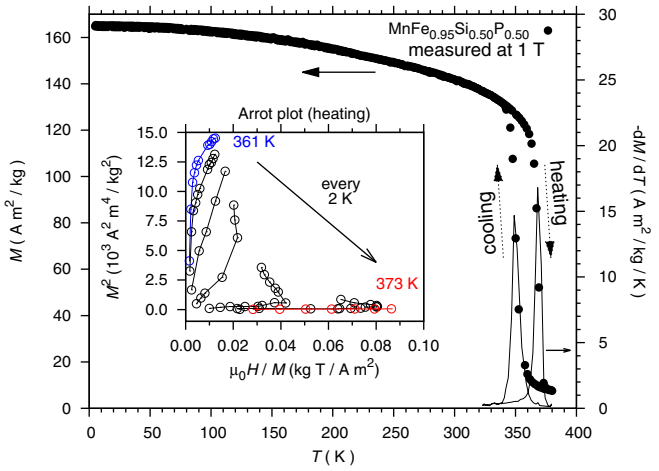

FIG. 1. (Left axis): Isofield magnetization data of $MnFe_{0.95}Si_{0.50}P_{0.50}$ (black tics) measured at $\mu_0 H = 1$ T between 5 and 380 K during cooling and heating. (Right axis): The (negative) first derivative of the corresponding magnetization data. Inset: Isothermal magnetization data measured between 0 and 5 T every 2 K between 361 K (blue tics) and 373 K (red tics) during heating are depicted in the Arrot plot. Lines between points are given as a guide to the eye. Error bars are smaller than the marker size.

external magnetic field between 0 and 5 T across the magnetic transition. A positive slope is observed in the Arrot plot [31] well below and above the magnetic transition, however, at the magnetic transition found at 369 K a negative slope is observed.

B. Structural characterization

The typical refinement for the x-ray diffraction pattern of $MnFe_{0.95}Si_{0.50}P_{0.50}$ is shown in Fig. 2. The majority of reflections can be indexed within the expected $P\bar{6}2m$ space group. A crystalline impurity phase related to the $(Mn, Fe)_3Si$

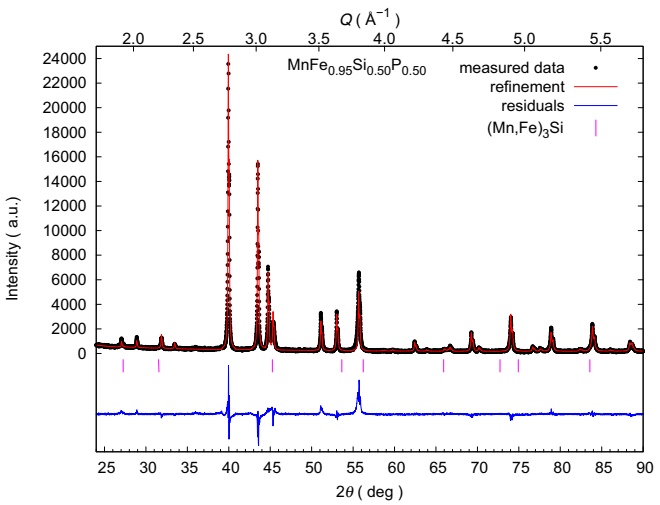

FIG. 2. X-ray diffraction pattern of $MnFe_{0.95}Si_{0.50}P_{0.50}$ (black points) measured experimentally at 295 K, the refinement (red line), the refinement residuals (blue line), and the reflection positions for the $(Mn,Fe)_3Si$ impurity phase (magenta tics).

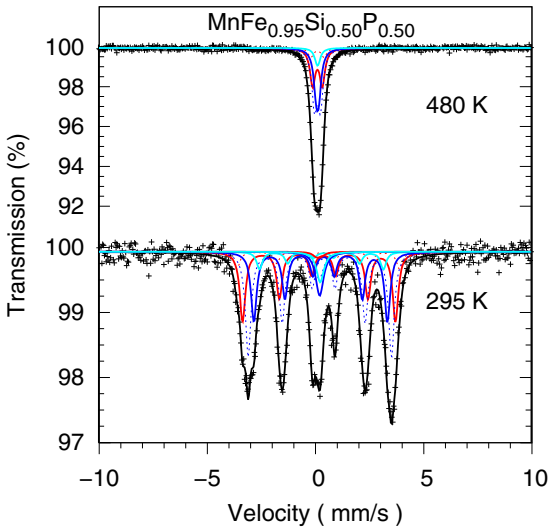

FIG. 3. ^{57}Fe-Mössbauer spectra of $MnFe_{0.95}Si_{0.50}P_{0.50}$ (black tics) measured in the ferromagnetic phase at 295 K (lower panel) and in the paramagnetic phase at 480 K (upper panel), the corresponding model (black line), and the components used in the model (color lines); see text for details.

stoichiometry (space group: $Fm\bar{3}m$) was found with a volume fraction of 7(2)%. The extracted lattice parameters of the main phase at $T = 295$ K are $a = 6.1949(2)$ Å and $c = 3.3040(1)$Å which corresponds to a unit cell volume of 109.814(5) Å^3. At $T = 450$ K the lattice parameters are $a = 6.0735(7)$ Å and $c = 3.4616(5)$ Å, which corresponds to a unit cell volume of 110.58(2) Å^3.

C. Hyperfine interactions characterization

The Mössbauer spectra measured on $MnFe_{0.95}Si_{0.50}P_{0.50}$ at 480 and 295 K are shown in Fig. 3. In the PM high-temperature phase a single broad absorption line is observed without traces of any additional Fe containing magnetic impurity phase. In the FM low-temperature phase a more complex absorption profile is observed that includes rather broad spectral lines, which indicates a hyperfine field distribution. Since P and Si are randomly distributed in the 2c and the 1b crystallographic positions this leads to five different Fe nearest neighbors. In such a case the experimental Mössbauer spectra are usually fitted with a model that weighs the contribution of each Fe environment using a binomial distribution [32]. A similar model is used in this case and a summary of the derived average hyperfine parameters, together with the linewidth, and the fraction of the magnetic phase are given in Table I. The extracted hyperfine magnetic field of the FM phase is 20.6(1) T. The average quadrupole splitting of the FM phase is −0.18(1) mm/s compared to 0.28(1) mm/s in the high temperature PM phase. A spurious PM phase with a phase fraction of 12(3)% is observed at low temperature with a different isomer shift and quadrupole splitting compared to the high-temperature PM phase. Notable is also the broad line with a linewidth of 0.41(1) mm/s for the impurity phase compared to the linewidth of the main phase that amounts to 0.30(1) mm/s.

TABLE I. Summary of the fit parameters extracted from the Mössbauer spectra using the model described in the text.

Compound	T (K)	⟨IS⟩ (mm/s)	⟨QS⟩ (mm/s)	$\langle\mu_0 H_{\rm hf}\rangle$ (T)	Γ (mm/s)	Phase	Fraction (%)
	480	0.11	0.28		0.29	PM	100
$MnFe_{0.95}Si_{0.50}P_{0.50}$	295	0.32	−0.18	20.6	0.32	FM	88
		0.22	0.09		0.41	PM	12

Experimental uncertainties: temperature: $T \pm 1$ K; average isomer shift: ⟨IS⟩ ± 0.01 mm/s; average quadrupole splitting: ⟨QS⟩ ± 0.01 mm/s; average hyperfine field $\langle\mu_0 H_{\rm hf}\rangle$: ±0.1 T
Line width: $\Gamma \pm 0.01$ mm/s; fraction: ±3%
PM/FM: paramagnetic/ferromagnetic

D. Lattice dynamics and thermodynamics characterization

The normalized (to unity) Fe DPS extracted from NIS measurements is depicted in Fig. 4. Both in the PM and in the FM state the DPS has the same overall shape, i.e., a pronounced peak is located between 20 and 30 meV, a phonon gap appears between 35 and 40 meV, a second peak shows up between 40 and 50 meV, a shoulder is seen close to 55 meV, and a phonon cutoff is observed at 60 meV. A pronounced downshift, 2 meV at 20 meV, of the main peak is observed in the FM state. This is corroborated by an increase in the Debye level from $5.4(2) \times 10^{-5}$ meV^{-3} in the FM to $7.6(3) \times 10^{-5}$ meV^{-3} in the PM state. All other features in the DPS remain (within the experimental accuracy) the same.

The density of phonon states, $g(E)$, provides direct access to a series of thermodynamic parameters [33]. The probability of the recoiless absorption, known as Lamb-Mössbauer factor, $f_{\rm LM} = \exp(-E_{\rm R} \int \frac{g(E)}{E} \frac{1+e^{-\beta E}}{1-e^{-\beta E}} dE)$ where $E_{\rm R} = 1.956$ meV is the recoil energy for ^{57}Fe and $\beta = \frac{1}{k_{\rm B}T}$, where $k_{\rm B}$ is the Boltzmann constant and T is the temperature at which the $g(E)$ is measured. The calculated $f_{\rm LM}$ for Fe in $MnFe_{0.95}Si_{0.50}P_{0.50}$ is 0.79(1) in the FM phase and 0.61(1) in the PM phase. From the Lamb-Mössbauer factor, the purely incoherent mean-square atomic displacement parameters, $\langle u^2\rangle = -\ln f_{\rm LM}/k^2$, where $k = 7.303$ Å^{-1} is the wave number of the resonant photons, is extracted. The Fe mean square atomic displacement is 44(1) pm^2 in the FM and 93(1) pm^2 in the PM state. The Fe specific mean-force constant $\langle F\rangle$ is also obtained from the expression $\langle F\rangle = M \int g(E) E^2 dE/\hbar^2$, where M is the mass of the resonant isotope, i.e., $M = 57$ amu. The obtained values are 191(1) N/m in the FM and 177(1) N/m in the PM state. The Fe specific Debye temperature, $\Theta_{\rm D}$, is obtained directly from Fe DPS using the formula $\Theta_{\rm D}^2 = 3/[k_{\rm B}^2 \int g(E) dE/E^2]$ valid in the high temperature limit. The obtained Debye temperature for Fe is 405(5) in the FM and 374(5) K in the PM phase. The vibrational contribution of Fe to the internal energy per atom may be calculated as $\langle E\rangle = 3/2 \int g(E) E \frac{e^{\beta E}+1}{e^{\beta E}-1} dE$. The extracted values are 80(2) meV in the FM and 131(2) meV in the PM phase. The average speed of sound, $v_{\rm s}$, is extracted from the Debye level, $\lim_{E\to 0} \frac{g(E)}{E^2}$, shown as inset to Fig. 4, using $\lim_{E\to 0} \frac{g(E)}{E^2} = \frac{M}{2\pi^2\hbar^3\rho v_{\rm s}^3}$ where ρ is the mass density and $\hbar$ is the Planck constant. The average speed of sound, $v_{\rm s}$, is 3.661(45) km/s in the FM and 3.267(43) km/s in the PM state. In addition, the vibrational entropy, $S_{\rm vib} = k_{\rm B} \int [\frac{\beta E}{2} \coth(\frac{\beta E}{2}) - \ln(2\sinh(\frac{\beta E}{2}))] g(E) dE$, may also be extracted given the density of vibrational states. The contribution of the Fe specific vibrations to the total entropy of the system is 2.88(9) $k_{\rm B}$/Fe atom in the FM and 4.69(5) $k_{\rm B}$/Fe atom in the PM state.

The normalized (to unity) x-ray generalized density of phonon states extracted from inelastic x-ray scattering measurements is depicted in Fig. 4. The x-ray generalized DPS has the same overall shape with the Fe specific DPS and follows the same trend with temperature, i.e., a softening by 2 meV of the main peak across the magnetic transition, whereas the high energy peak in the DPS is insensitive to the magnetic transition.

IV. DISCUSSION

A. The impurity phase

In addition to the main $MnFe_{0.95}Si_{0.50}P_{0.50}$ phase an impurity phase with general chemical formula $(Mn,Fe)_3Si$ was identified using both x-ray diffraction and ^{57}Fe Mössbauer spectroscopy. The amount of the impurity phase extracted from Mössbauer spectroscopy, 12%, is slightly larger compared to the amount of the impurity phase extracted from x-ray diffraction, 7%. This might indicate that a part of the impurity phase is either in amorphous/nanocrystalline form or with high degree of disorder. This would result in a limited correlation length, thus, it does not show up fully in the x-ray diffraction data. This observation is also supported by the broad linewidth of the impurity phase compared to the main phase extracted by Mössbauer spectroscopy.

The magnetic characterization in $(Mn,Fe)_3Si$ systems is reported in previous studies [34–36]. The magnetic ordering temperature in the $(Mn,Fe)_3Si$ system varies between 30 K in Mn_3Si and 800 K in Fe_3Si and depends strongly on the Mn to Fe ratio. In the Mössbauer spectrum measured in this study the impurity phase is paramagnetic at room temperature. Moreover, no additional magnetic transition relevant to the impurity phase appears in our magnetometry measurements. This indicates that the impurity phase present in our samples is Mn rich, with general stoichiometry $Mn_{2+x}Fe_{1-x}Si$ where $0 < x < 1$.

Although the Mn to Fe ratio drastically changes the magnetic order in $(Mn,Fe)_3Si$ it hardly affects the lattice dynamics. The mass homology relation in isostructural systems indicates that the energy of the vibrational modes varies as a function of the lattice parameters ratio and the nuclear mass ratio [37]. The nuclear masses of Mn and Fe are practically the same. Both Mn_3Si and Fe_3Si crystallize in the same crystal structure, and the lattice parameters between Mn_3Si and Fe_3Si are very close, 5.722 and 5.650 Å [38], respectively. As a result, the density of phonon states in Fe_3Si is expected to be practically the same, an energy shift less than 0.4% is expected according

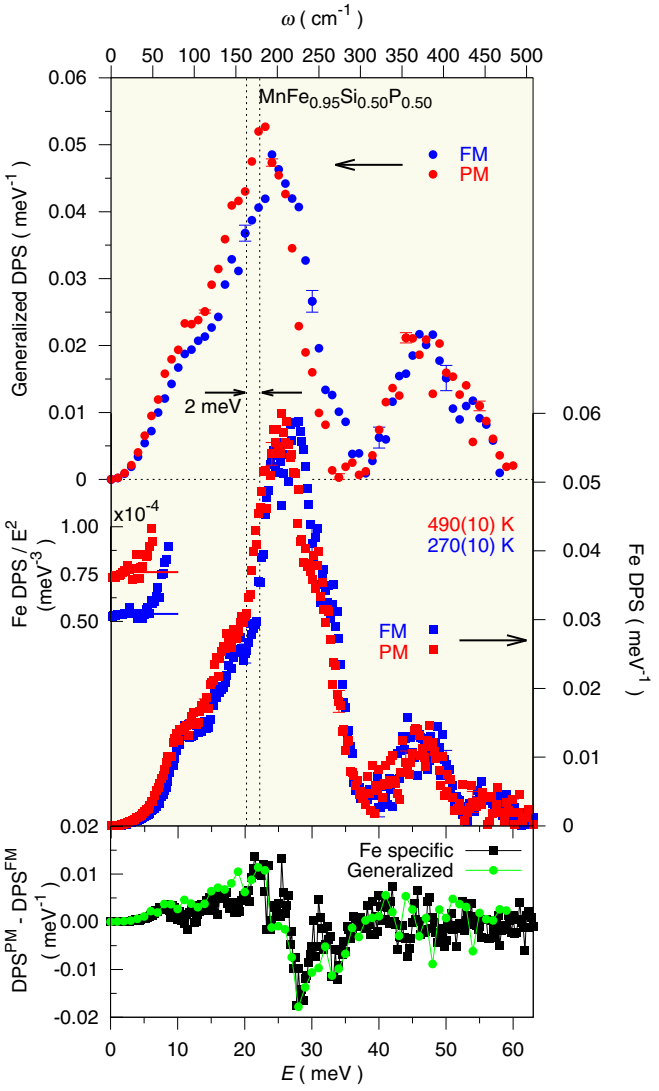

FIG. 4. (Middle panel): The Fe specific density of phonon states (DPS) measured on $MnFe_{0.95}Si_{0.50}P_{0.50}$ in the ferromagnetic (FM) state at 250(20) K (blue squares) and in the paramagnetic state (PM) at 490(20) K (red squares) using nuclear inelastic scattering. Inset: The same data in the Debye setting, DPS/E^2, are shown below 10 meV. The solid lines correspond to the Debye level extracted by fitting the data with a constant between 1 and 5 meV. (Top panel): The x-ray generalized DPS measured on the same sample and at the same temperature using inelastic x-ray scattering; see text. Characteristic error bars are given. (Lower panel): The difference between the DPS measured in the PM state and the DPS measured in the FM state using both nuclear inelastic scattering (black marker) and inelastic x-ray scattering (green marker).

to mass homology relation, with the corresponding in Mn_3Si. The phonon dispersion relation and the density of phonon states have been studied both theoretically and experimentally in Fe_3Si [39,40]. The main phonon peak in the density of phonon states of Fe_3Si appears as a sharp doublet between 40 and 42 meV. Such a sharp peak is practically absent, both in our nuclear inelastic scattering data as well as in our inelastic x-ray scattering data and does not occur in the phonon gap of $MnFe_{0.95}Si_{0.50}P_{0.50}$. A negligibly small but still nonzero Fe density of phonon states around 40 meV, indicative of a broad spurious peak may be correlated with the impurity phase. A density of phonon states with broad features is indeed attributed to disordered systems [41]. Nevertheless, it is clear that such a broad spurious background does not change across the magnetic transition. Notably, the lack of any kind of transition relevant to the impurity phase, i.e., structural, magnetic, in the studied temperature range indicate that the impurity phase does not contribute in the magnetocaloric properties.

B. Order of magnetic transition in $MnFe_{0.95}Si_{0.50}P_{0.50}$

In $MnFe_{0.95}Si_{0.50}P_{0.50}$ a pronounced magnetic transition from a FM to a PM state with slope $-dM/dT = 16(1)$ $Am^2/kg/K$ occurs at 351(1) K (for cooling) with a thermal hysteresis of 17 K between cooling and heating curves. The thermal hysteresis and the sharpness of the transition are typical features of nucleation and growth and indicate that the type of the magnetic transition is of first order. In order to further verify the order of the transition, magnetization measurements with varying magnetic field were carried out. The negative slope observed in the isothermal plots of M^2 as function of $\mu_0 H/M$, in the Arrot plot (inset of Fig. 1), verify that the magnetic transition is of first order [42].

C. Fe local environment in $MnFe_{0.95}Si_{0.50}P_{0.50}$

Mössbauer spectra on $(Mn,Fe)_2(P,Si)$ compounds have already been reported for various Mn to Fe and Si to P ratios [43], as well as with As in the place of Si [32]. In all studies a binomial distribution that weighs the contribution of the different iron sites is used, resulting in an average value for the isomer shift, the quadrupole splitting, and the hyperfine magnetic field. In this study we used the same model [32,43,44] to fit the data. In the previous Mössbauer studies on the As containing samples the average values for the quadrupole splitting were constrained. As a result Sougrati *et al.*, [44] observed a significant decrease in isomer shift from the ferromagnetic to the paramagnetic phase, a decrease that according to the authors could not be supported by other evidences. In this study we let the quadrupole splitting vary as a free parameter. The average value for the quadrupole splitting in the FM phase extracted in this study, $-0.18(1)$ mm/s, is close to the constrained value, -0.11 mm/s, in the $MnFeAs_{0.50}P_{0.50}$. For more details on a negative quadrupole splitting the reader may follow Ref. [45]. In the PM phase the extracted average quadrupole splitting is shifted more than the resonance linewidth, i.e., about 0.3 mm/s, to 0.28(1) mm/s, compared to value extracted in the FM state, $-0.18(1)$ mm/s. This observation, combined with the relatively large change in the average isomer shift from 0.32(1) mm/s in the FM phase to 0.11(1) mm/s in the PM phase, indicates that the local environment of Fe changes significantly by the magnetic transition.

D. Lattice dynamics, Fe vibrations, and thermodynamics in $MnFe_{0.95}Si_{0.50}P_{0.50}$

Inelastic x-ray scattering is a useful tool in order to obtain the x-ray generalized density of phonon states without involving magnetic excitations. As expected from their atomic numbers the Fe and Mn contribution is dominant in the x-ray

generalized DPS. This is clearly seen in Fig. 4, where a direct comparison between the x-ray generalized and the Fe specific density of phonon states is evident. The main peak in the x-ray generalized density of phonon states and in the Fe specific density of phonon states show exactly the same trend across the magnetic transition, see lower panel in Fig. 4. This clearly indicates that the magnetic transition primarily affects the Fe vibrational modes, whereas the Mn vibrational modes are essentially not affected by the magnetic transition.

Absolute values in both the vibrational eigenvalues and eigenvectors are provided *per se* using nuclear inelastic scattering, which is not the case for inelastic x-ray scattering. Thus, only the Fe specific thermodynamic properties are extracted herein and are given for future reference. The average speed of sound in $MnFe_{0.95}Si_{0.50}P_{0.50}$ extracted from the long-wavelength limit of the Fe specific DPS is higher than 3 km/s, both in the FM and in the PM state. A similar value was found in $Mn_{5-x}Fe_xSi_3$ compounds [14]. Moreover, such a value is typical for common solids. The Fe specific Debye temperature, 403(5) K, extracted in the FM state in this study is very close to the Debye temperature, 420 K, extracted using calorimetry in the FM state of the parent Fe_2P compound [46]. All in all, $MnFe_{0.95}Si_{0.50}P_{0.50}$ behaves as a typical metallic compound except for the change in the density of vibrational states across the magnetic transition.

The change in the Fe vibrational entropy between the FM and the PM state extracted in this study is 1.81(10) k_B/Fe atom. However, this value includes a contribution due to a temperature change between 270(10) K and 490(10) K and a contribution due to the change in the DPS at the magnetic transition. The Fe vibrational entropy at 490 K calculated using the Fe DPS measured at 270 K is 4.54 k_B/Fe atom. As a result, the vibrational entropy change only due to the change in the DPS at the magnetic transition is 0.15(5) k_B/Fe atom. In the unit cell there are on average 2.85 Fe atoms with a mass of 57 amu each. Thus, the change in Fe vibrational entropy across the magnetic transition due to the change in the DPS is 62(21) J/K/kg. This value is within the error bar the same with the value, 58 J/K/kg, extracted from calorimetry experiments [47] on similar compounds. This indicates that the iron vibrational entropy change across the magnetic transition is dominant. The relatively large error bar in the vibrational entropy, which is related mainly with the uncertainty in the temperature extracted by applying the detailed balance, does not allow us to precisely calculate the difference between the vibrational and the total entropy change. Nevertheless, the extracted vibrational entropy across the magnetic transition is notably higher than the typical magnetic entropy change observed in these compounds across the magnetic transition, of about 10 J/K/kg, under the application of 1 T external magnetic field.

In $(Mn,Fe)_2(Si,P)$ compounds no crystallographic transition with a symmetry change nor a jump in the volume occur. This is well documented [22,48,49] and confirmed in this study since no global change in the generalized density of phonon states is observed. As a result, a change in the configurational entropy across the magnetic transition may be neglected. Instead, a sizable change of almost 4% in the c/a ratio (in this study the c/a is 0.533 at 295 K and 0.569 at 450 K) is observed in these compounds [50]. A notable change in the c/a ratio without a volume change in hexagonal symmetry systems manifest usually under externally applied pressure. Such transitions are known as Lifshitz transitions [51] and are usually related with electronic topological transitions [52]. Lately, thermally stimulated electronic topological transitions are also reported [53]. Such an electronic topological transition in $(Mn,Fe)_2(Si,P,B)$ which involves changes in the electron density around Fe was recently suggested using x-ray absorption spectroscopy and high-resolution x-ray diffraction [54]. It is therefore plausible that the changes (i) in the local environment, which is quantified in the average isomer shift and the average quadrupole splitting, and (ii) in the lattice dynamics, which is quantified in the energy downshift of the main peak in the DPS, is providing another indication for an electronic topological transition concomitant to the magnetic transition. Whether such an electronic topological transition is coupled to the magnetic transition remains to be further investigated by a combination of first principle calculations as well as advanced microscopic magnetic [55] and electronic [56] measurements.

V. CONCLUSION

Lattice dynamics characterization in $MnFe_{0.95}Si_{0.50}P_{0.50}$ using nuclear inelastic scattering by ^{57}Fe and inelastic x-ray scattering show that the main peak, around 20 meV, in the density of vibrational states, which is essentially of Fe character, substantially softens, by 2 meV, across the first-order magnetic transition, whereas higher energy vibrational modes are insensitive to the magnetic transition. Such an effect could not be attributed to a usual phase transition since neither a symmetry change nor an abrupt volume change is observed at the magnetic transition. The majority of the extracted thermodynamic properties do not capture this effect. The magnetic entropy change is not sufficient to cover the Fe vibrational entropy change and another source of entropy should be taken into account. The thermally stimulated change in the Fe local environment observed by hyperfine interactions characterization indicate that an electronic topological transition may be concomitant to the magnetic transition and could contribute notably in the coupling between magnetic and elastic degrees of freedom.

ACKNOWLEDGMENTS

The European Synchrotron Radiation Facility is acknowledged for provision of synchrotron radiation beam time at ID18 and ID28. We thank: Dr. A. I. Chumakov, Dr. R. Rüffer for helpful discussions and J.-P. Celse for technical assistance during the beamtime at ID18/ESRF, and Dr. A. Bosak for helpful discussions and D. Gambetti for technical assistance during the beamtime at ID28/ESRF. The technical assistance of A. J. E. Lefering is acknowledged during sample preparation and macroscopic characterization. D.B. acknowledges financial support from the Industrial Partnership Program (IPP-I28) of Foundation for Fundamental Research on Matter (FOM) (The Netherlands) and BASF New Business.

[1] E. Brück, J. Phys. D: Appl. Phys. **38**, R381 (2005).
[2] T. Christiaanse and E. Brück, Metall. Mater. Trans. E **1**, 36 (2014).
[3] S. Nikitin, G. Myalikgulyev, A. Tishin, M. Annaorazov, K. Asatryan, and A. Tyurin, Phys. Lett. A **148**, 363 (1990).
[4] V. K. Pecharsky and K. A. Gschneidner, Jr., Phys. Rev. Lett. **78**, 4494 (1997).
[5] R. Wäppling, L. Häggström, T. Ericsson, S. Devanarayanan, E. Karlsson, B. Carlsson, and S. Rundqvist, J. Solid State Chem. **13**, 258 (1975).
[6] S. Fujieda, A. Fujita, and K. Fukamichi, Appl. Phys. Lett. **81**, 1276 (2002).
[7] A. Planes, L. M. nosa, and M. Acet, J. Phys.: Condens. Matter **21**, 233201 (2009).
[8] X. Bohigas, J. Tejada, E. del Barco, X. X. Zhang, and M. Sales, Appl. Phys. Lett. **73**, 390 (1998).
[9] M.-H. Yu, L. H. Lewis, and A. R. Moodenbaugh, J. Appl. Phys. **93**, 10128 (2003).
[10] H. Yibole, F. Guillou, L. Zhang, N. H. van Dijk, and E. Brück, J. Phys. D: Appl. Phys. **47**, 075002 (2014).
[11] A. Fujita, S. Fujieda, Y. Hasegawa, and K. Fukamichi, Phys. Rev. B **67**, 104416 (2003).
[12] M. E. Gruner, W. Keune, B. Roldan Cuenya, C. Weis, J. Landers, S. I. Makarov, D. Klar, M. Y. Hu, E. E. Alp, J. Zhao *et al.*, Phys. Rev. Lett. **114**, 057202 (2015).
[13] L. Jia, J. R. Sun, H. W. Zhang, F. X. Hu, C. Dong, and B. G. Shen, J. Phys.: Condens. Matter **18**, 9999 (2006).
[14] M. Herlitschke, B. Klobes, I. Sergueev, P. Hering, J. Perßon, and R. P. Hermann, Phys. Rev. B **93**, 094304 (2016).
[15] H. Fujii, T. Hokabe, K. Eguchi, H. Fujiwara, and T. Okamato, J. Phys. Soc. Jpn **51**, 414 (1982).
[16] B. Huliyageqi, Y.-x. Geng, Y.-j. Li, and O. Tegus, J. Korean Phys. Soc. **63**, 525 (2013).
[17] H. Wada, T. Takahara, K. Katagiri, T. Ohnishi, K. Soejima, and K. Yamashita, J. Appl. Phys. **117**, 172606 (2015).
[18] D. T. C. Thanh, E. Brück, N. T. Trung, J. C. P. Klaasse, K. H. J. Buschow, Z. Q. Ou, O. Tegus, and L. Caron, J. Appl. Phys. **103**, 07B318 (2008).
[19] N. T. Trung, Z. Q. Ou, T. J. Gortenmulder, O. Tegus, K. H. J. Buschow, and E. Brück, Appl. Phys. Lett. **94**, 102513 (2009).
[20] E. Brück, M. Ilyn, A. Tishin, and O. Tegus, J. Magn. Magn. Mater. **290–291**, 8 (2005).
[21] P. Roy, E. Brück, and R. A. de Groot, Phys. Rev. B **93**, 165101 (2016).
[22] N. H. Dung, L. Zhang, Z. Q. Ou, L. Zhao, L. van Eijck, A. M. Mulders, M. Avdeev, E. Suard, N. H. van Dijk, and E. Brück, Phys. Rev. B **86**, 045134 (2012).
[23] Z. Klencsár, Hyperfine Interact. **217**, 117 (2013).
[24] M. Seto, Y. Yoda, S. Kikuta, X. W. Zhang, and M. Ando, Phys. Rev. Lett. **74**, 3828 (1995).
[25] W. Sturhahn, T. S. Toellner, E. E. Alp, X. Zhang, M. Ando, Y. Yoda, S. Kikuta, M. Seto, C. W. Kimball, and B. Dabrowski, Phys. Rev. Lett. **74**, 3832 (1995).
[26] R. Rüffer and A. I. Chumakov, Hyperfine Interact. **97-98**, 589 (1996).
[27] V. Kohn and A. Chumakov, Hyperfine Interact. **125**, 205 (2000).
[28] M. Krisch and F. Sette, *Inelastic X-Ray Scattering from Phonons* (Springer, Berlin, Heidelberg, 2007), pp. 317–370.
[29] A. Bosak and M. Krisch, Phys. Rev. B **72**, 224305 (2005).
[30] D. Bessas, R. E. Simon, K. Friese, M. Koza, and R. P. Hermann, J. Phys.: Condens. Matter **26**, 485401 (2014).
[31] A. Arrott, Phys. Rev. **108**, 1394 (1957).
[32] R. P. Hermann, O. Tegus, E. Brück, K. H. J. Buschow, F. R. de Boer, G. J. Long, and F. Grandjean, Phys. Rev. B **70**, 214425 (2004).
[33] M. Y. Hu, T. S. Toellner, N. Dauphas, E. E. Alp, and J. Zhao, Phys. Rev. B **87**, 064301 (2013).
[34] V. Niculescu, K. Raj, T. J. Burch, and J. I. Budnick, Bull. Am. Phys. Soc. **20**, 587 (1975).
[35] H. J. Al-Kanani, J. G. Booth, J. W. Cable, and J. A. Fernandez-Baca, J. Appl. Phys. **76**, 6359 (1994).
[36] J. Leitão, Y. Xinmin, L. Caron, and E. Brück, J. Alloys Compd. **520**, 52 (2012).
[37] H. R. Schober and W. Petry, *Lattice Vibrations* (Wiley-VCH Verlag GmbH, Berlin, 2006).
[38] S. Yoon and J. Booth, Phys. Lett. A **48**, 381 (1974).
[39] S. Dennler and J. Hafner, Phys. Rev. B **73**, 174303 (2006).
[40] O. G. Randl, G. Vogl, W. Petry, B. Hennion, B. Sepiol, and K. Nembach, J. Phys.: Condens. Matter **7**, 5983 (1995).
[41] A. R. Overy, A. Simonov, P. A. Chater, M. G. Tucker, and A. L. Goodwin, Phys. Status Solidi B **254**, 1600586 (2017).
[42] B. Banerjee, Phys. Lett. **12**, 16 (1964).
[43] X. F. Miao, Y. Mitsui, A. I. Dugulan, L. Caron, N. V. Thang, P. Manuel, K. Koyama, K. Takahashi, N. H. van Dijk, and E. Brück, Phys. Rev. B **94**, 094426 (2016).
[44] M. T. Sougrati, R. P. Hermann, F. Grandjean, G. J. Long, E. Brück, O. Tegus, N. T. Trung, and K. H. J. Buschow, J. Phys.: Condens. Matter **20**, 475206 (2008).
[45] D. C. Cook, Z. Naturforsch., A: Phys. Sci. **51**, 368 (1996).
[46] O. Beckman, L. Lundgren, P. Nordblad, P. Svedlindh, A. Törne, Y. Andersson, and S. Rundqvist, Phys. Scr. **25**, 679 (1982).
[47] F. Guillou, H. Yibole, N. van Dijk, and E. Brück, J. Alloys Compd. **632**, 717 (2015).
[48] X. F. Miao, L. Caron, Z. Gercsi, A. Daoud-Aladine, N. H. van Dijk, and E. Brück, Appl. Phys. Lett. **107**, 042403 (2015).
[49] M. F. J. Boeije, M. Maschek, X. F. Miao, N. V. Thang, N. H. van Dijk, and E. Brück, J. Phys. D: Appl. Phys. **50**, 174002 (2017).
[50] F. Guillou, G. Porcari, H. Yibole, N. van Dijk, and E. Brück, Adv. Mater. **26**, 2671 (2014).
[51] I. M. Lifshitz, JETP **11**, 1130 (1960).
[52] K. Glazyrin, L. V. Pourovskii, L. Dubrovinsky, O. Narygina, C. McCammon, B. Hewener, V. Schünemann, J. Wolny, K. Muffler, A. I. Chumakov *et al.*, Phys. Rev. Lett. **110**, 117206 (2013).
[53] F. C. Yang, J. A. Muñoz, O. Hellman, L. Mauger, M. S. Lucas, S. J. Tracy, M. B. Stone, D. L. Abernathy, Y. Xiao, and B. Fultz, Phys. Rev. Lett. **117**, 076402 (2016).
[54] M. F. J. Boeije, P. Roy, F. Guillou, H. Yibole, X. F. Miao, L. Caron, D. Banerjee, N. H. van Dijk, R. A. de Groot, and E. Brück, Chem. Mater. **28**, 4901 (2016).
[55] N. Biniskos, S. Raymond, K. Schmalzl, A. Schneidewind, J. Voigt, R. Georgii, P. Hering, J. Persson, K. Friese, and T. Brückel, Phys. Rev. B **96**, 104407 (2017).
[56] L. J. P. Ament, M. van Veenendaal, T. P. Devereaux, J. P. Hill, and J. van den Brink, Rev. Mod. Phys. **83**, 705 (2011).